Memoirs of the Faculty of Engineering, Nagoya University
Vol. 30, No. 1 (1978) — Research Report —

ANALYSIS OF DYNAMIC CHARACTER OF ONE-DIMENSIONAL DOMAIN WALL MOTION BIASED BY STATIC IN-PLANE FIELD

TOSHITAKA FUJII,* TAKASHI SHINODA, SHIGERU SHIOMI, and SUSUMU UCHIYAMA

Department of Electrical Engineering

(Recieved May 30, 1978)

Abstract

The dynamic character of domain wall motion was investigated for a one-dimensional planar wall by solving numerically Gilbert equation of motion. It is confirmed from the numerical analysis that the application of the in-plane field is useful to improve the dynamic character, especially in the high drive field region. Despite the analysis was made for a virtual one-dimensional wall, the results seem to explain qualitatively the experiments in garnet bubbles. Besides we solved the wall motion analytically by making an approximation with a simplified wall profile under the biased in-plane field, from which all properties obtained by the numerical analysis can easily be derived.

1. Introduction

It is observed in many bubble domains in garnet films that the wall velocity exhibits the breakdown or the saturation in the high drive field region.[1] This unfavorable phenomenon for computer memory application is generally referred to as the "*dynamic conversion*",[2] which is briefly interpreted as follows: In a moving wall, a force originates from the gyrotropic nature of spin exerts on the magnetization inside the wall so as to convert into a complicated structure of the spin configuration having a large inertia mass, whereby the wall velocity can no longer increase even when the drive field further increases. A mean to improve the dynamic character in high speed wall motion suppressing the dynamic conversion is attained by either applying an in-plane field externally[3] or utilizing an in-plane

* Present address, School of Electrical Engineering and Electronics, Toyohashi University of Technology, Toyohashi, Aichi 440

anisotropy field due to the orthorhombic anisotropy in garnet platelets.[4] The theoretical considerations, however, have mostly been made on the latter case: The effectiveness of the in-plane anisotropy field was first pointed out by Thiele[5] for one-dimensional wall within the scheme of the Walker's theory[6] and recently calculated by Schlömann[7] for more realistic two-dimensional wall with the finite thickness, whereas systematic studies on that of external in-plane field have apparently not yet been published to date, except the work of de Leeuw *et al.*[3] who analysed it under the condition that the in-plane field is sufficiently large compared to the stray field which arises from the surface charge at the center of the wall *i. e.* $H_{in-plane} \geqslant 8M$, where M: the saturation magnetization. The authors[8] previously investigated through numerical analysis the effect of the in-plane field on one-dimensional wall motion under the application of arbitrary magnitude of the in-plane field as a direct extension of the work of Schryer and Walker.[9] However, since we used in [8] such a small q-value as 0.047, which is the same that used in [9] (the q-value is defined by $q=k/2\pi M^2$: the ratio of the uniaxial anisotropy energy perpendicular to the film plane to the energy due to the demagnetizing field of film), the substantial problem was involved to compare to bubble experiments, because the q-value of bubble materials must be larger than unity. In this respect we made again numerical computation for $q>1$ according to similar prescription of [8]. In the present paper we summerize the computed results of $q=2$ as well as those of $q=0.047$ which were partially described in [8] in detail. In order to obtain the qualitative understanding on the general character of biased wall motion, we evolved an approximate analysis using a simplified wall profile which is available for large q-value as actually used in bubble device.

2. Outline of Numerical Computation Procedures

As the detail of the numerical computation procedures to obtain the wall motion by integrating Gilbert equation of motion was given in [8] and [9], we describe here the brief explanation on it. As shown in Fig. 1 (upper), we introduce the Cartesian coordinate (x, y, z) to define the location of wall and the polar coordinate (θ, ϕ) to define the magnetization vector $\vec{M}=(M_x, M_y, M_z)=M$ $(\sin\theta\cos\phi, \sin\theta\sin\phi, \cos\theta)$. A planar 180°-Bloch wall lies on the yz-plane, whose y-coordinate being $y=S(t)$ at the moment t. Taking the uniaxial medium whose easy direction parallel to the z-axis, the drive field to displace the wall toward y-direction is the field parallel to the z-direction H_z, and the in-plane field H_b is supposed to be the field applied in the plane perpendicular to H_z, *i. e.*, $H_b=(H_x, H_y)$ in the xy-plane, which only acts on the wall so as to deform the wall configuration. We consider here the case when the in-plane field is applied either on the wall surface (H_x) or normal to the wall surface (H_y). Fig. 1 (below) illustrates how to compute the wall motion biased by the in-plane field $H_{x,y}$. Since it is impossible to analytically express the initial wall configuration biased by $H_{x,y}$, we determined it by computing the equation of motion [see eq. (2)] until the solution under the application of $H_{x,y}$ tends to the stationary state. The wall motion under the drive field of a constant amplitude H_z applied at the moment $t=0$ is then obtained by using the same computation routine. To treat analysis in a general way, we use hereafter the dimensionless quantities for the time t, the length y, the field strength

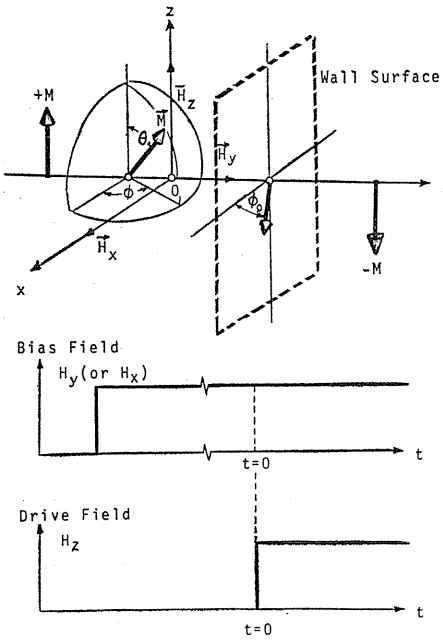

Fig. 1. Coordinate System for computation of the domain wall motion (upper) and schematic representation for the application of the inplane field, $H_{x,\,y}$, and the drive field, H_z (lower).

$H_{x,y,z}$, and the wall velocity $v=dS/dt$ as,

$$T\equiv\gamma\cdot 2\pi Mt,\quad Y\equiv\frac{y-S(t)}{\Delta_0},\quad h_{x,\,y,\,z}\equiv\frac{H_{x,\,y,\,z}}{H_c},\quad \text{and}\quad \hat{v}\equiv\frac{dY}{dT}=\frac{v}{2\pi\gamma M\Delta_0},\qquad (1)$$

where γ is the gyromagnetic ratio, Δ_0 is the width parameter of the standing still wall, and $H_c\equiv 2\pi\alpha M$ (α: the phenomenological damping parameter) is so-called the Walker field, the critical field below which the stationary wall motion is realized. By the use of eq. (1), Gilbert equation with respect to θ and ϕ is expressed as,

$$\frac{\partial\theta}{\partial T}+\alpha\sin\theta\frac{\partial\phi}{\partial T}=\alpha\begin{Bmatrix}-h_x\sin\phi\\ h_y\cos\phi\end{Bmatrix}-\sin\theta\sin 2\phi+2q\frac{1}{\sin\theta}\cdot\frac{\partial}{\partial Y}\left(\sin^2\theta\frac{\partial\phi}{\partial Y}\right)\qquad (2\,a)$$

$$\alpha\frac{\partial\theta}{\partial T}-\sin\theta\frac{\partial\phi}{\partial T}=-q\sin 2\theta-\alpha h_z\sin\theta+\alpha\begin{Bmatrix}h_x\cos\theta\cos\phi\\ h_y\cos\theta\sin\phi\end{Bmatrix}-\sin 2\theta\sin^2\phi$$
$$+q\left[2\frac{\partial^2\theta}{\partial Y^2}-\sin 2\theta\left(\frac{\partial\phi}{\partial Y}\right)^2\right]\qquad (2\,b)$$

In eqs. (2a) and (2b), the variable parameters other than the field $h_{x,\,y,\,z}$ are α and q. The numelical integration of eqs. (2a) and (2b), was carried out by means of ordinary Runge-Kutta method and found to generally become instable when we use either large $h_{x,\,y}$ or large q-value. In order to avoid the instability for a large $h_{x,\,y}$, the computation was made by changing $h_{x,\,y}$ stepwise to its final value. For a large q-value it is necessary to choose appropriate small time and, eventually spatial increments of ΔT and ΔY, as well as the large integration interval in both

sides of the wall, $[-Y_0, Y_0]$. These quantities used are: $\Delta T=0.25$, $\Delta Y=0.1$ and $Y_0=7$ to 14 for $q=0.047$, and $\alpha=0.01$; $\Delta T=0.006$ to 0.012, $\Delta Y=0.1$, and $Y_0=14$ for $q=2$ and $\alpha=0.05$.

3. Numerical Analysis

3. 1. Domain Wall Configuration under In-plane Field

Vella Coleiro[10] observed in garnet bubbles the oscillation of the wall displacement and hence its time derivative, the wall velocity, from stroboscopic measurement of wall motion when the wall is driven by high drive field exceeded a critical value and showed that the period of the oscillation agrees well with that predicted by Schryer and Walker[9] for one-dimensional wall. The wall velocity in the oscil-

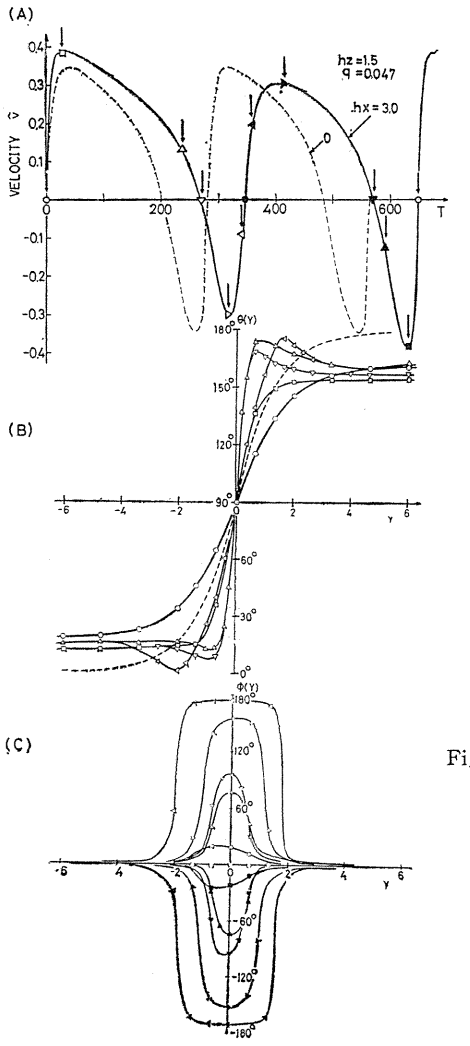

Fig. 2. (A) Oscillation of the wall velocity $\hat{v}(T)$ as a function of the reduced time, T for $q=0.047$ and $\alpha=0.01$, under the field condition of $h_z=1.5$, and $h_x=3$. Dashed curve is the case of no in-plane field. (B) and (C) are the domain wall profile in terms of $\theta(Y)$ and $\phi(Y)$, respectively, at some moments marked by the arrows in (A).

latory mode results in an abrupt decrease on the average of time. To begin with we shall show how the in-plane field affects on the domain wall configuration in the oscillatory mode. Fig. 2 to Fig.5 are four examples of the computed results, in which Fig. 2 and Fig. 3 are the cases for the small q-value of 0.047, and Fig. 4 and Fig.5 those for the large q-value of 2, Fig. 2 and Fig. 4, and Fig. 3 and Fig. 5 are respectively the cases when h_x and h_y are applied. The field strength $h_{x,y,z}$ used are written in the figures. The top of each figure shows the temporal change of $\hat{v}(T)$ as a function of T, the middle and the bottom being respectively the domain wall profiles in terms of θ and ϕ at some typical moments of the oscillation as pointed by the arrows in the figures. From these figures the wall

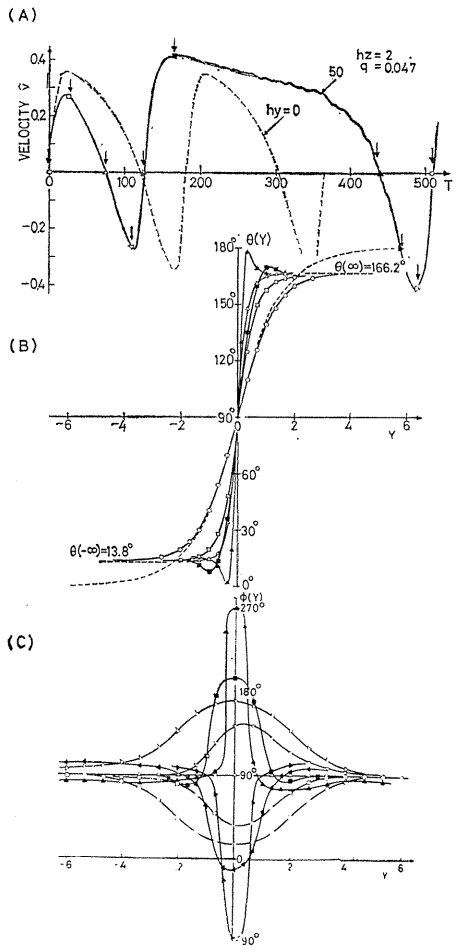

Fig. 3. (A) $\hat{v}(T)$ for $q=0.047$, and $\alpha=0.01$ under the field condition of $h_z=2$, and $h_y=50$, (B) and (C) the wall profile in terms of θ (Y), and ϕ (Y), respectively.

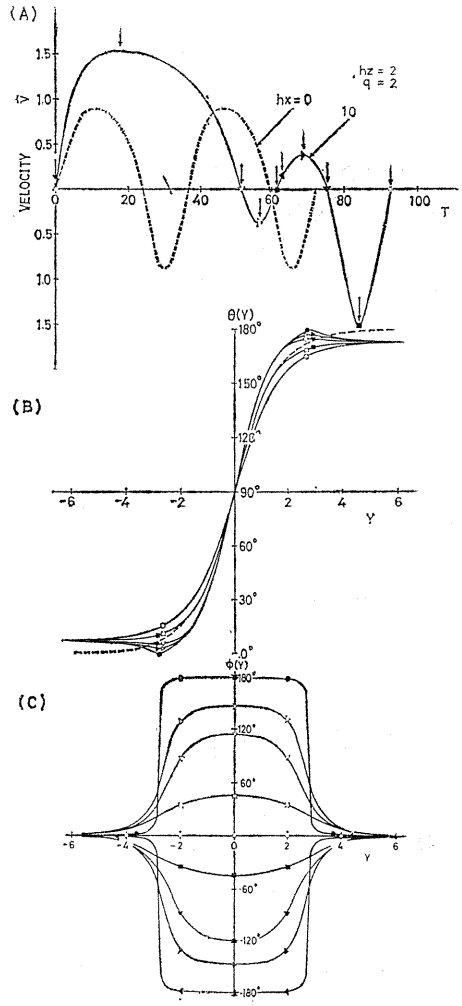

Fig. 4. (A) $\hat{v}$(T) for $q=2$, and $\alpha=0.05$ under the field condition of $h_z=2$, and $h_x=10$, (B) and (C) the wall profile in terms of $\theta(Y)$ and $\phi(Y)$, respectively.

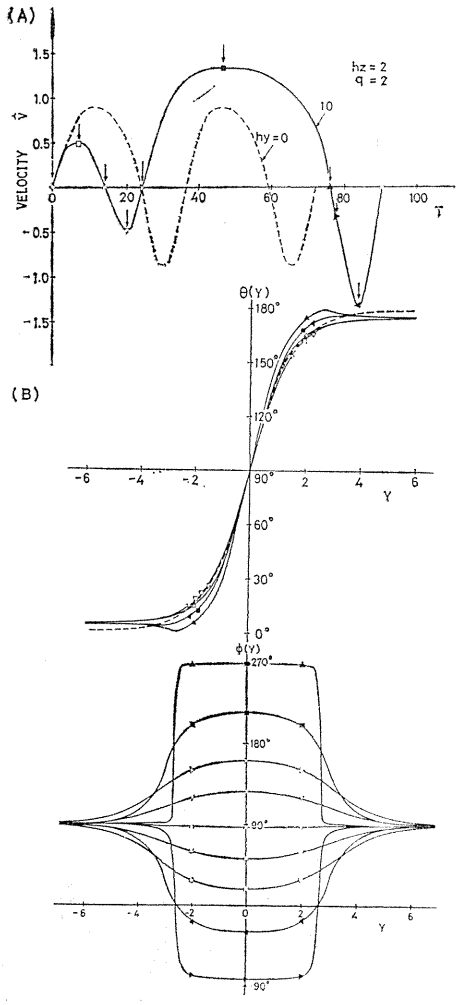

Fig. 5. (A) $\hat{v}(T)$ for $q=2$ and $\alpha=0.05$ under the field condition of $h_z=2$, and $h_y=10$, (B) and (C) are the domain wall profile in terms of $\theta(Y)$ and $\phi(Y)$, respectively.

configuration is subjected to a complicated change by the application of the in-plane field in comparison with that of no in-plane field, where θ keeps the same functional dependence at rest [$\theta=2\tan^{-1}\exp(Y)$] and ϕ is substantially constant regardless of Y. It is further recognized that the wall configuration of $q=2$ is simpler than that of $q=0.047$. This is due to the facts that with increasing q-value, (i) the wall contraction during wall motion is small, and (ii) the contribution from the exchange energy increases [see eq. (2)], so that the spatial variation of wall is retained. If, though numerical computation might be more difficult, one computes for a large q-value as actually used in bubble materials ($q=5\sim10$), the wall configuration will be much simpler as shown in Fig. 14.

3. 2. Effect of In-plane Field on Wall Velocity

On comparing the solid curves with in-plane field and the dashed ones without in-plane field in the top figures of Fig. 2 to Fig. 5, the period and the amplitude

of the oscillation of $\hat{v}(T)$ are subjected to modulation by the application of the in-plane field as well. This is understood from eqs. (2a) and (2b) as the following way: We consider first the case where the in-plane field is absent. The magnetization inside the wall experiences the torque to rotate around the z-axis by h_z, $\partial\phi/\partial T$, which gives rise to the demagnetizing field due to the free poles appearing along the wall width. The demagnetizing field generates the torque, $\sin\theta\sin 2\phi$, which exerts on the magnetization to rotate upwards so as to decrease θ, $-\partial\theta/\partial T$. This torque is the motive torque to push the wall toward the y-direction. When an in-plane field is applied, the motive torque depends, in addition to the demagnetizing torque, on that due to the in-plane field, $\sin\theta\sin 2\phi+\begin{Bmatrix}\alpha h_x\sin\phi\\ -\alpha h_y\cos\phi\end{Bmatrix}$ [Strictly speaking, the third contribution from the exchange torque, $-2q\dfrac{1}{\sin\theta}\cdot\dfrac{\partial}{\partial Y}\left(\sin\dfrac{\partial\phi}{\partial Y}\right)$, must be taken into account, because of the spatial variation of θ]. Thus comparing to the case of no in-plane field, the period and the wall velocity in the oscillatory mode are increased or decreased according to whether both torques act in the same direction to enhance them or the opposite direction to diminish them, depending on the orientation of the magnetization ϕ. It is considered that under appropriate field condition, the period becomes infinity resulting in the cease of precession, $\partial\phi/\partial T=0$, this means that the oscillatory mode is converted into the stationary mode. In the absence of in-plane field, the stationary mode is realized only when the drive field is smaller than the Walker field, [$h_z<1$], while by applying the in-plane field, it is expected that the stationary mode is realized even when $h_z>1$.

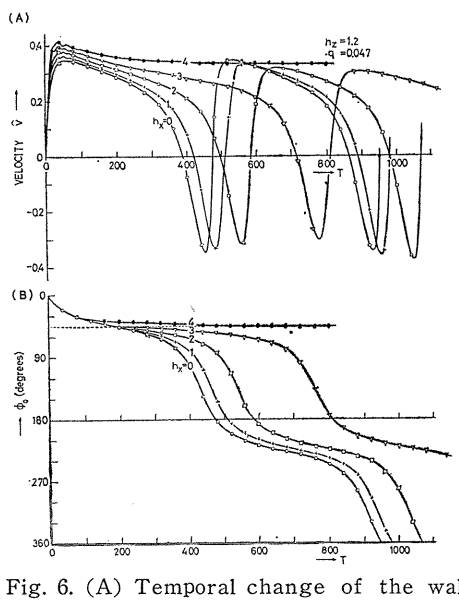

Fig. 6. (A) Temporal change of the wall velocity $\hat{v}$ and (B) the azimuthal angle at the center of the wall surface $\phi_0=\phi(0)$ *vs.* the reduced time T for $q=0.047$, and $\alpha=0.01$, where $h_z=1.2$ and h_x is changed as a parameter.

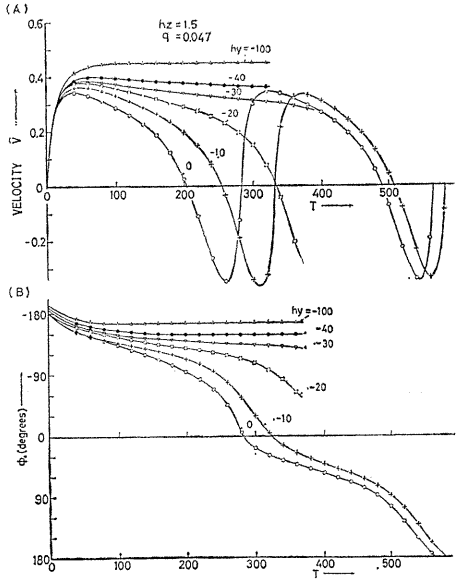

Fig. 7. $\hat{v}$ (A) and ϕ_0 (B) *vs.* T for $q=0.047$, and $\alpha=0.01$, where $h_z=1.5$ and h_y is changed as a parameter.

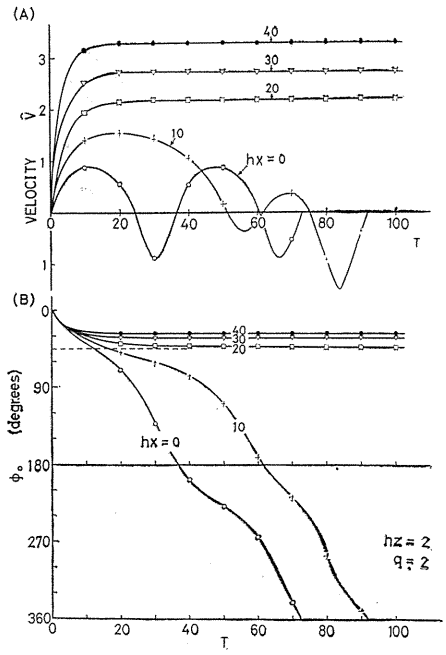

Fig. 8. $\hat{v}$ (A) and ϕ_0 (B) *vs.* T for $q=2$, and $\alpha=0.05$, where $h_z=2$ and h_x is changed as a parameter.

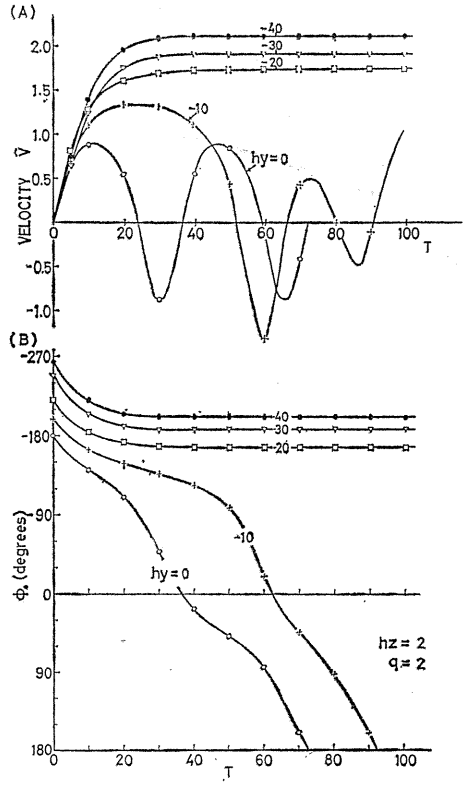

Fig. 9. $\hat{v}$ (A) and ϕ_0 (B) *vs.* for $q=2$, and $\alpha=0.05$, where $h_z=2$, and h_y is changed as a parameter.

In order to confirm this consideration, computation was made by changing various combinations of h_z and $h_{x,y}$. Fig. 6 to Fig. 9 show four examples of the computed results for the wall velocity $\hat{v}(T)$ and the magnetization orientation at the center of the wall, $\phi_0 \equiv \phi(0)$, in which Fig. 6 and Fig. 7 are the cases for $q=0.047$, and Fig. 8 and Fig. 9 are those for $q=2$, where the curves are drawn for a fixed h_z and several in-plane field $h_{x,y}$ as a parameter. In any case the period of the wall oscillation is lengthened with increasing the in-plane field and finally tends to the stationary wall motion with a constant velocity, $\hat{v}_s$, when the in-plane field exceeds a certain strength, in accordance with above expectation. It can be shown that $\hat{v}_s$ is the maximum wall velocity to be achieved under the given drive field strength, which is very desirable for the application of high speed wall motion. Fig. 10 ($q=0.047$) and Fig. 11 ($q=2$) are the dependences of $\hat{v}$ on $h_{x,y}$ keeping h_z constant, where for the oscillatory mode, the peak velocity $\hat{v}_p$ and the time-average velocity, $\langle\hat{v}\rangle_t = \frac{1}{T}\int_0^T \hat{v}(\tau)d\tau$, are plotted. From these figures, the wall velocity increases with increasing in-plane field, the effect of the in-plane field on the wall velocity is more stronger for $q=2$ than $q=0.047$: $\hat{v}_s$ increases approximately linearly to $h_{x,y}$ for $q=2$, while $\hat{v}_s$ tends to the saturation in high $h_{x,y}$ for $q=0.047$. $\langle\hat{v}\rangle_t$ in both cases increases approximately proportionally to $h^2{}_{x,y}$ as has observed in experi-

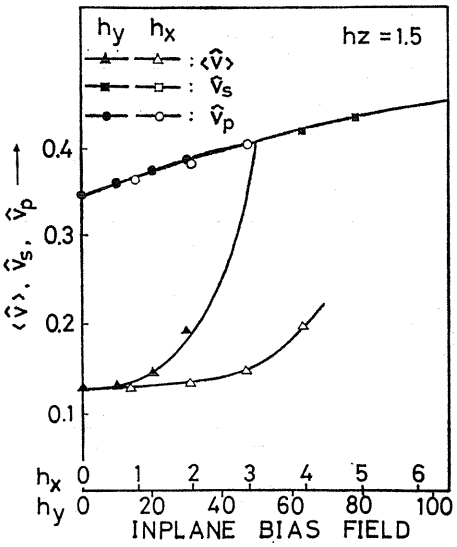

Fig. 10. Dependence of the wall velocity $\hat{v}$ on the in-plane field $h_{x,y}$ for $q=0.047$, and $\alpha=0.01$, where h_z is chosen as a parameter. $\hat{v}_s$, $\langle\hat{v}\rangle_t$, $\hat{v}_p$ stand for respectively the velocity in the stationary mode, the time-average and the peak velocities in the oscillatory mode. Dashed curves are the results calculated by the approximate analysis in § 4.

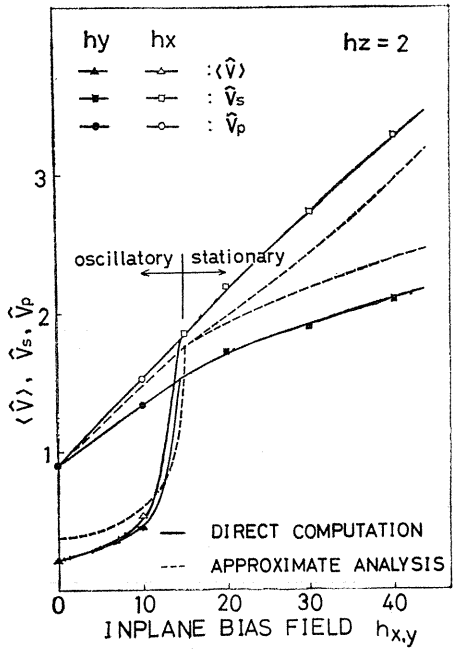

Fig. 11. Dependence of $\hat{v}$ on $h_{x,y}$ for $q=2$, and $\alpha=0.05$, where h_z is chosen as a parameter. Various marks are the same that used in Fig. 10.

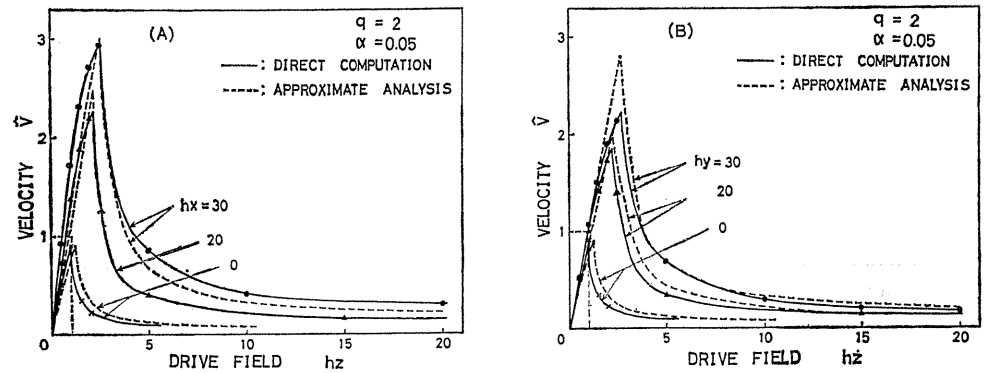

Fig. 12. Dependence of $\hat{v}$ on h_z for $q=2$, and $\alpha=0.05$, where the in-plane fields h_x (A) and h_y (B) are chosen as a parameter. Dashed curves are the results calculated by the approximate analysis in § 4.

ments[3,11]. It is further noting that $\hat{v}$ has the dependence of the direction of the in-plane field: The most effective direction is the x-direction for $q=2$, while the y-direction for $q=0.047$. Fig. 12 shows, on the contrary, the dependence of $\hat{v}$ on h_z for choosing $h_{x,y}$ as a parameter, in which the left side where $\hat{v}$ increases,

corresponds to the stationary mode and the right side where $\hat{v}$ decays out, the oscillatory mode. Let the maximum drive field under a fixed in-plane field to maintain the stationary mode and the velocity at this field call as the critical field, h_{crit}, and the critical velocity, $\hat{v}_{crit}$, respectively, which correspond to the Walker field ($h_z=1$) and the Walker velocity in the case of no in-plane field, respectively. As seen from this figure, such available parameters as the wall mobility, $\mu_w=(\partial\hat{v}_s/\partial h_z)_{h_x,\,y}$, h_{crit}, and $\hat{v}_{crit}$ are monotonically increased with increasing $h_{x,\,y}$, among which $\hat{v}_{crit}$ and h_{crit} of Fig. 12 (A) are plotted as a function of h_x in Fig. 13. Both increase linearly at least in the range of computed h_x in agreement with the analysis of de Leeuw.[7]

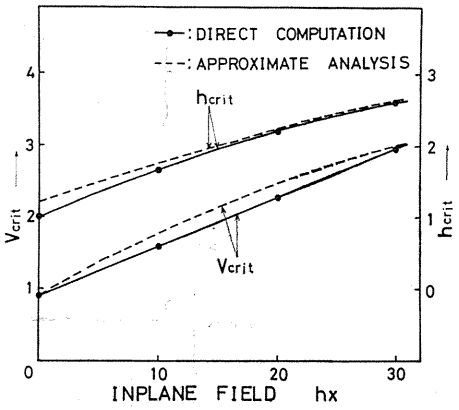

Fig. 13. Relationship of the critical velocity, $\hat{v}_{crit}$, and the critical field, h_{crit}, against the in-plane field, h_x, in Fig. 12 (A), where dashed curves are calculated by the approximate analysis in § 4.

4. Approximate Analysis

As has already described in the last paragraph of Section 3. 1., the wall profile biased by the in-plane field can be approximated by the curves drawn in Fig. 14 for large q-value (compare Fig. 14 and Fig. 4), In this case, apart from tedious numerical computation, one can discuss wall dynamics analytically and can explain easily the various properties in the foregoing section.

The analytical expressions of the variations of θ and ϕ in Fig. 14 are, respectively,

$$\theta(y,\ T)=\begin{cases}\dfrac{\pi}{2}+\dfrac{\pi-\theta_0}{\Delta(t)}[y-s(t)], & |y-s(t)|\leq\Delta(t)/2\\ \pi-\theta_0, & y-s(t)>\Delta(t)/2\\ \theta_0, & y-s(t)<-\Delta(t)/2\end{cases}\qquad(3\,a)$$

$$\phi(y,\ t)=\begin{Bmatrix}0\\ \pi/2\end{Bmatrix}+\Phi(t)\left[u\left(y-s(t)+\frac{1}{2}\Delta(t)\right)-u\left(y-s(t)-\frac{1}{2}\Delta(t)\right)\right],\qquad(3\,b)$$

where $s(t)$, $\Delta(t)$, $\Phi(t)$ are the y-coordinate of the wall center, the wall width, and the amplitude of $\phi(y,\ t)$ which fluctuates with time, at the moment t, respectively. θ_0 denotes the inclination of the magnetization with respect to the z-axis and $u(x)=1$, for $x\geq 0$; $u(x)=0$, for $x<0$, the unit step function. If $h_{x,\,y}\gg h_z$, θ_0 is given by eq. (4) :

$$\theta_0 = \begin{cases} \sin^{-1}\dfrac{MH_x}{2K} = \sin^{-1}\dfrac{h_x}{2q}, & (4\,a) \\ \sin^{-1}\dfrac{MH_y}{2(K+2\pi M^2)} = \sin^{-1}\dfrac{h_y}{2(q+1)}. & (4\,b) \end{cases}$$

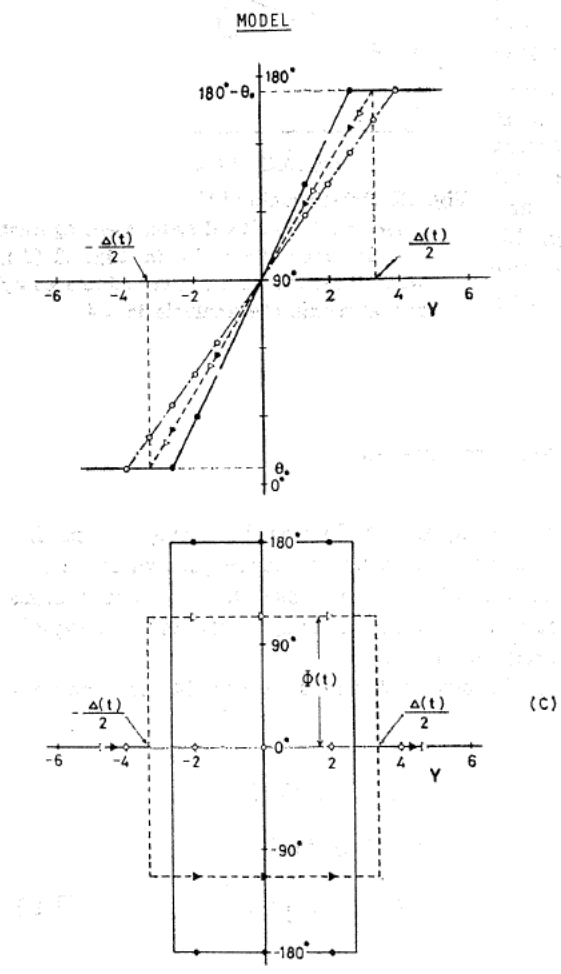

Fig. 14. A model of the domain wall profile biased by the in-plane field used for the approximate analysis.

According to Slonczewski,[12] Gilbert equation is expressed in the integral form as,

$$\int\left(\frac{\partial\theta}{\partial t}+\alpha\frac{\partial\phi}{\partial t}\sin\theta\right)\sin\theta\,dy=\frac{\gamma}{M}\cdot\frac{\delta\sigma}{\delta\phi}, \qquad (5\,a)$$

$$\int\left(\frac{\partial\phi}{\partial t}\sin\theta-\alpha\frac{\partial\theta}{\partial t}\right)dy=\frac{\gamma}{M}\cdot\frac{\delta\sigma}{\delta\theta}, \qquad (5\,b)$$

where $\frac{\delta\sigma}{\delta\phi}=\frac{\partial\sigma}{\partial\phi}-\frac{\partial}{\partial y}\left(\frac{\partial\sigma}{\partial\left(\frac{\partial\phi}{\partial y}\right)}\right)$ is the functional derivative with respect to ϕ and σ the internal energy to be considered which consists of following five contributions: The uniaxial anisotropy energy, the energy due to the demagnetizing field across the wall width, the potential energies due to the drive and the in-plane fields, and the exchange energy;

$$\sigma=\int\Big[K\sin^2\theta+2\pi M^2\sin^2\theta\sin^2\phi-MH_z\cos\theta - \begin{Bmatrix}MH_x\sin\theta\cos\phi\\ MH_y\sin\theta\sin\phi\end{Bmatrix}+A\left\{\left(\frac{\partial\theta}{\partial y}\right)^2+\sin^2\theta\left(\frac{\partial\phi}{\partial y}\right)^2\right\}\Big]dy. \tag{6}$$

Substituting eqs. (3) and (6) into eq. (5) and integrating over y, we get eq. (7) by the use of non-dimensional quantities of eq. (1) [Although the integrands involve such singular functions as $u(x)$ and $du(x)/dx$, the singularities do not affect the result because the divergences at two singular points of $y=s(t)\pm\frac{1}{2}\Delta(t)$ cancel each other].

$$(\pi-2\theta_0)\dot{s}\cos\theta_0-\frac{1}{4}\alpha\dot{\phi}(\pi-2\theta_0+\sin 2\theta_0)$$

$$=\frac{1}{4}\eta(T)\Big[(\pi-2\theta_0+\sin 2\theta_0)\sin 2\phi\pm 4\alpha\begin{Bmatrix}h_x\\ h_y\end{Bmatrix}\cos\theta_0\begin{Bmatrix}\sin\\ \cos\end{Bmatrix}\phi, \tag{7a}$$

$$\alpha(\pi-2\theta_0)^2\dot{s}+2\dot{\phi}\cos\theta_0=2\eta(T)\alpha h_z\cos\theta_0, \tag{7b}$$

where $\eta(T)=\Delta(T)/\Delta_0$ is the wall contraction, $\dot{s}$ is $\hat{v}(T)$ in the previous sections, the dot $\cdot$ denotes the derivative with respect to the reduced time T, $\partial/\partial T$. On solving eqs. (7a) and (7b) with respect to $\dot{s}$ and $\dot{\phi}$, and using an approximation of $\pi-2\theta_0+\sin 2\theta_0\simeq\pi$, we have,

$$\dot{s}=\frac{\eta\cos\theta_0}{4(\pi-2\theta_0)\Lambda}\Big[\pi\sin 2\phi+\pi^2\alpha^2h_z\pm 4\alpha\begin{Bmatrix}h_x\\ h_y\end{Bmatrix}\cos\theta_0\begin{Bmatrix}\sin\\ \cos\end{Bmatrix}\phi\Big], \tag{8a}$$

$$\dot{\phi}=\frac{\alpha h_z\cos^2\theta_0}{\Lambda}\Big[1-a\sin 2\phi\mp b\begin{Bmatrix}\sin\\ \cos\end{Bmatrix}\phi\Big], \tag{8b}$$

where

$$\Lambda\equiv\cos^2\theta_0+\frac{\alpha^2}{8}\pi(\pi-2\theta_0),$$
$$a\equiv\frac{1}{8h_z}\cdot\frac{\pi(\pi-2\theta_0)}{\cos^2\theta_0},\quad b\equiv\frac{h_{x,y}}{2h_z}\cdot\frac{(\pi-2\theta_0)}{\cos\theta_0}, \tag{9}$$

and the upper and the lower signs in eq. (8) correspond to the cases when the in plane field of h_x and h_y are applied, respectively.

4. 1. Stationary Mode

The condition for the stationary wall motion is obtained by putting $\dot{\phi}=0$ in eq.

(7):

$$\sin 2\phi=\frac{1}{a}\mp\frac{b}{a}\begin{Bmatrix}\sin\\ \cos\end{Bmatrix}\phi=\frac{8h_z\cos^2\theta_0}{\pi(\pi-2\theta_0)}\mp\frac{4\alpha h_{x,y}}{\pi}\cos\theta_0\begin{Bmatrix}\sin\\ \cos\end{Bmatrix}\phi. \tag{10}$$

This is the extension of the Walker condition,

$$\sin 2\phi=h_z, \tag{11}$$

for the absence of the in-plane field, that is, if we put $h_{x,y}=0$ (and hence $\theta_0=0$), then we get,

$$\sin 2\phi=\frac{8}{\pi^2}h_z(\simeq 0.8106h_z)\equiv\tilde{h}_z, \tag{12}$$

which agrees with eq. (11) except the numerical constant of $8/\pi^2$. The stationary wall velocity $\hat{v}_s$ is obtained readily from eq. (7b) as,

$$\hat{v}_s\equiv\dot{s}|_{\phi=0}=\eta\frac{2h_z\cos\theta_0}{(\pi-2\theta_0)^2}=\frac{\pi^2}{4}\eta\frac{\tilde{h}_z\cos\theta_0}{(\pi-2\theta_0)^2}. \tag{13}$$

This relation can also be derived from more rigorous formula of the energy conservation of moving wall[8],

$$\alpha\hat{v}_s\int_{-\infty}^{\infty}\left[\left(\frac{\partial\theta}{\partial Y}\right)^2+\sin^2\theta\left(\frac{\partial\phi}{\partial Y}\right)^2\right]dy=2\alpha h_z\cos\theta_0, \tag{14}$$

by substituting eqs. (3a) and (3b). The wall contraction η is determined to make the comparison with the Walker solution[6], $\hat{v}_s=h_z/(1+q^{-1}\sin^2\phi)^{1/2}$ and $\hat{v}_s=(1/4)\eta\tilde{h}_z$ [put $\theta_0=0$ in eq. (13)]. Thus we have,

$$\eta=4/(1+q^{-1}\sin^2\phi)^{1/2} \tag{15}$$

The factor 4 of the numerator in eq. (15) arises from the approximation of eqs. (3a) and (3b).

4. 2. Oscillatory Mode

The quantities to determine the dynamic character such as the instantaneous velocity $\hat{v}(T)=\dot{s}$, the orientation of the magnetization $\phi(T)$, and the period of the wall oscillation, $F=\int_0^{2\pi}\dot{\phi}^{-1}d\phi$, can be obtained by solviog the simultaneous differential equations of eqs. (7a) and (7b). From the viewpoint of engineering application, however, most interesting may be the time-average of the wall velocity $\langle\dot{s}\rangle_t=\langle\hat{v}\rangle_t$, which is determined from eq. (7a) as,

$$\langle\hat{v}\rangle_t=\frac{\cos\theta_0}{4(\pi-2\theta_0)}\left[\pi\langle\eta\sin 2\phi\rangle_t+\pi\alpha^2h_z\langle\eta\rangle_t\right.$$
$$\left.\pm 4\alpha\begin{Bmatrix}h_x\\ h_y\end{Bmatrix}\cos\theta\begin{Bmatrix}\langle\eta\cos\phi\rangle_t\\ \langle\eta\cos\phi\rangle_t\end{Bmatrix}\right], \tag{16}$$

where $\langle f\rangle_t$ stands for the time-average of $f(T)$, which is calculated by using eq. (7b) as,

$$<f>_t=\lim_{F\to\infty}\frac{1}{F}\int_0^F f(\tau)d\tau$$

$$=\frac{\int_0^{2\pi}\frac{f(\psi)}{\dot{\psi}}d\psi}{\int_0^{2\pi}\frac{d\psi}{\dot{\psi}}}=\frac{\int_0^{2\pi}\frac{f(\psi)d\psi}{1-a\sin 2\psi\pm b\left\{\begin{matrix}\cos\\ \sin\end{matrix}\right\}\psi}}{\int_0^{2\pi}\frac{d\psi}{1-a\sin 2\psi\pm b\left\{\begin{matrix}\cos\\ \sin\end{matrix}\right\}\psi}}. \tag{17}$$

5. Comparison with Numerical Analysis and Discussion

First let us compare the approximate analysis of § 4 to the direct computation of Gilbert equation of § 3. Since the approximation is valid for large q-value, the comparison was made only for $q=2$ as shown by the dashed lines in Fig. 11 to Fig. 13. It is seen from these figures that both agree fairly well though $q=2$ is not yet sufficiently large to use the approximation. Next let us show how main conclusions of § 3 can be explained from the approximate analysis of § 4.

(a) The in-plane field acts on the magnetization so as to suppress the precession, so that the stationary wall motion is realized, even when the drive field exceeds the Walker field.

The critical field $h_{\rm crit}$ is determined by putting $(\partial h_z/\partial\phi)_{h_{x,y}}=0$ in eq. (7a). If we neglect the effect of the wall contraction η, $h_{\rm crit}$ becomes,

$$h_{\rm crit}=\frac{(\pi-2\theta_0)}{8\cos^2\theta_0}\left[\sin 2x\pm\frac{4\alpha h_{x,y}}{\pi}\cos\theta_0\left\{\begin{matrix}\sin\\ \cos\end{matrix}\right\}x\right], \tag{18 a}$$

where

$$\left\{\begin{matrix}\cos\\ \sin\end{matrix}\right\}x=\frac{1}{2}\left[\pm\frac{h_{x,y}}{\pi}\cos\theta_0\pm\left(\left(\frac{h_{x,y}}{\pi}\cos\theta_0\right)^2+2\right)^{1/2}\right], \tag{19}$$

thus the critical velocity $\hat{v}_{\rm crit}$ is from eq. (13) as,

$$\hat{v}_{\rm crit}=\frac{8h_{\rm crit}}{(\pi-2\theta_0)^2}\cos\theta_0. \tag{18 b}$$

According to eq. (7), $h_{\rm crit}$ and $\hat{v}_{\rm crit}$ should change proportionally to $h_{x,y}$. It seems, however, to be rather difficult to derive these relations explicitly from eqs. (7a) and (7b) because θ_0 is dependent on $h_{x,y}$ in the manner as eq. (4a) or (4b). The result of straightfoward computation of $h_{\rm crit}$ and $\hat{v}_{\rm crit}$ are shown in Fig. 13, which are nearly proportionally to $h_{x,y}$ in accordance with eq. (8).

(b) The wall mobility $\tilde{\mu}_w=(\partial\hat{v}_s/\partial\tilde{h}_z)_{h_{x,y}}$ is also improved by the application of the in-plane field (see Fig. 12).

$\tilde{\mu}_w$ is calculated readily from eq. (12) as,

$$\tilde{\mu}_w=\frac{\pi^2}{4}\eta\frac{\cos\theta_0}{(\pi-2\theta_0)^2}. \tag{20}$$

Under the condition of $q \gg 1$ and $\alpha h_{x,y} \ll q$, eq. (18) reduces to,

$$\tilde{\mu}_w \simeq 1 + \frac{2}{\pi} \cdot \frac{h_{x,y}}{q}, \tag{20'}$$

which represents that $\tilde{\mu}_w$ should increase proportionally to $h_{x,y}$ but at the same time the effect of the in-plane field is weakened inversely to q.

(c) The time-average of the wall velocity $<\hat{v}>_t$ in the oscillatory mode changes approximately proportionally to the square of the in-plane field.

For the constants a and b in eq. (8), $1 \gg a \gg b$ holds under the ordinary field condition, so that eq. (14) is approximated by,

$$<\hat{v}>_t \simeq \frac{\pi \cos\theta_0}{(\pi - 2\theta_0)} <\sin 2\psi>_t$$

$$\simeq \frac{\pi \cos\theta_0}{(\pi - 2\theta_0)} \cdot \frac{\int_0^{2\pi} \sin 2\psi d\psi [1 + a \sin 2\psi \mp b \left\{ \begin{matrix} \cos \\ \sin \end{matrix} \right\} \psi]}{\int_0^{2\pi} [1 + a \sin 2\psi \mp b \left\{ \begin{matrix} \cos \\ \sin \end{matrix} \right\} \psi] d\psi}$$

$$= \frac{\pi^2}{16 h_z \cos^2\theta_0} \simeq \frac{\pi^2}{16 h_z} (1 + \theta_0^2) \simeq \frac{\pi^2}{16 h_z} \left(1 + \frac{\alpha^2}{4q^2} h_{x,y}^2\right). \tag{21}$$

(d) The stationary velocity $\hat{v}_s$ is the maximum velocity which can be achieved under a given drive field.

From eq. (7b), the wall velocity is generally expressed by,

$$\dot{s} = \hat{v}_s = \frac{2\phi_0 \cos\theta_0}{\alpha(\pi - 2\theta_0)^2}, \tag{22}$$

so that we get $\dot{s} \leq \hat{v}_s$ because of $\dot{\phi} > 0$ in the oscillatory mode [because the precession direction is anti-clockwise for positive h_z], or $\dot{\phi} = 0$ in the stationary mode.

As shown above, the dynamic character of wall motion is found to be improved by the application of the in-plane field, under which the wall velocity increases, regardless whether the wall moves stationary or oscillatory. This fact can also be interpreted from another viewpoint of the wall configuration. Since, from eq. (14), the stationary veloity $\hat{v}_s$ is related to the reciprocal of the exchange energy, *i. e.*, $E_{ex} = A \int_{-\infty}^{\infty} dY [(\partial\theta/\partial Y)^2 + \sin^2\theta (\partial\phi/\partial Y)^2]$, it is expected that the wall is converted into the wall having smaller E_{ex} by the in-plane field. Fig. 15 is an example of the wall configurations in the stationary mode for four different in-plane fields, For the spatial variation inside the wall, $|\partial\theta/\partial Y| \gg |\sin\theta (\partial\phi/\partial Y)|$ holds, so that E_{ex} is determined mainly by $\partial\theta/\partial Y \simeq (\pi - 2\theta_0)/\Delta$, which decreases with increasing the in-plane field, thus E_{ex} also decreases.

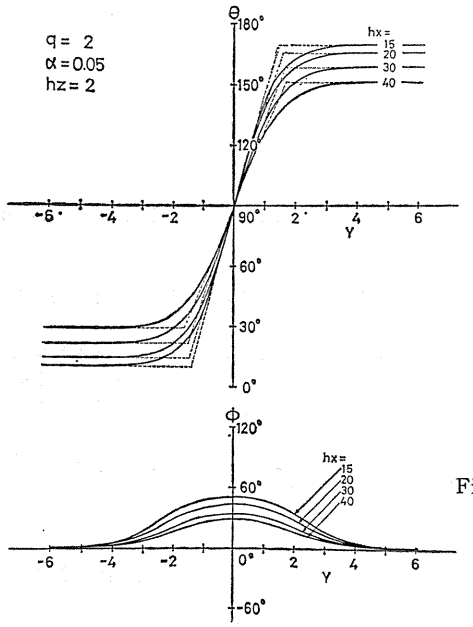

Fig. 15. Domain wall profiles of $\theta(Y)$ and $\phi(Y)$ in the stationary mode for $q=2$, and several in-plane fields h_x.

6. Concluding Remarks

In this paper we have investigated the wall dynamics on a virtual one-dimensional wall, which utterly ignores two-dimensional structure of wall such as the twisted spin arrangement along the film thickness and the virtical Bloch line, the co-mixture of Néel segment in a Bloch wall. When a wall once moves, these two-dimensional structures are apt to be converted into more complicated three-dimensional structure such as the horizontal Bloch line. This is the theoretical basis of the dynamic conversion.[2] Since the wall shape of bubble domain is not planar but circular or elliptic, the wall is inherently three-dimensional. Nevertheless it is considered that one-dimensional wall is still useful to survey the nature of domain wall motion as in suggested from experimental fact that the Walker oscillation was observed in bubble domain.[10] Indeed most of bubble experiments concerning the effect of the in-plane field[2, 11] may, to some extent, be interpreted by the present work.

Acknowledgement

The authors would like to thank Dr. S. Tsunashima of our laboratory for his kind and stimulating discussion throughout the study and Mr. A. Emura, the Japanese Agency for Space Development, for performing the numerical analysis and preparing the program for computer analysis. Computation was made on the FACOM 230-75 System of the Computation Center, Nagoya University. This work was partly sup-

ported by the Grant-in-Aid for the Scientific Research from the Ministry of Education.

References

(1) G. P. Vella-Coleiro, F. B. Hagedorn, Y. S. Chen, and S. L. Blank: Appl. Phys. Letters, **22** (1973) 324.
(2) F. B. Hagedorn: J. Appl. Phys., **45** (1974) 3129.
(3) R. J. Rijnierse, and F. H. de Leeuw: *AIP Conf. Proc.*, No. 18 Part 1 (1973) 199. F. H. de Leeuw: IEEE Trans. on Magnetics, **MAG-9** (1974) 614.
(4) W. T. Stacy, A. B. Voermans, and H. Logmans: Appl. Phys. Letters, **29** (1976) 817. D. J. Breed, W. T. Stacy, A. B. Voermans, H. Logmans, and A. M. J. van der Heijden: IEEE Trans. on Magnetics, **MAG-13** (1977) 1087. R. Wolfe, R. C. LeCraw, S. L. Blank, and R. D. Pierce: Appl. Phys. Letters, **29** (1976) 815.
(5) A. A. Thiele: cited by F. B. Hagedorn in *AIP Conf. Proc.*, No. 5 Part 1 (1971) 72.
(6) L. R. Walker: cited by J. F. Dillon, Jr. *Magnetism*, ed. G. T. Rado and H. Suhl (Academic Press, New York, 1963) Vol. 3, p. 450.
(7) E. Schlömann: J. Appl. Phys., **47** (1976) 1142.
(8) A. Emura, T. Fujii, S. Shiomi, and S. Uchiyama: IEEE Trans. on Magnetics, **MAG-13** (1977) 1169.
(9) N. L. Schryer, and L. R. Walker: J. Appl. Phys., **45** (1974) 5406.
(10) G. P. Vella-Coleiro: Appl. Phys. Letters: **29** (1976) 445, IEEE Trans. on Magnetics, **MAG-13** (1977) 1163.
(11) R. M. Josephs, and B. F. Stein: *AIP Conf. Proc.*, No. 18 Part 1 (1973) 227. T. Ideshita, Y. Fukushima, S. Honda, and T. Kusuda; IEEE Trans. on Magnetics, MAG-13 (1977) 1166.
(12) J. C. Slonczewski: Intern. J. Magnetism, **2** (1972) 85.